The Adiabatic Pole-to-Pole Overturning Circulation

CHRISTOPHER L. WOLFE AND PAOLA CESSI

Scripps Institution of Oceanography, University of California, San Diego, La Jolla, California

ABSTRACT

The adiabatic pole-to-pole cell of the residual overturning circulation (ROC) is studied in a two-hemisphere, semienclosed basin, with a zonally reentrant channel occupying the southernmost eighth of the domain. Three different models of increasing complexity are used: a simple, analytically tractable zonally averaged model; a coarse-resolution numerical model with parameterized eddies; and an eddy-resolving general circulation model. Two elements are found to be necessary for the existence of an adiabatic pole-to-pole cell: 1) a thermally indirect, wind-driven overturning circulation in the zonally reentrant channel, analogous to the Deacon cell in the Antarctic Circumpolar Current (ACC) region, and 2) a set of outcropping isopycnals shared between the channel and the semienclosed region of the Northern Hemisphere. These points are supported by several computations varying the domain geometry, the surface buoyancy distribution, and the wind forcing. All three models give results that are qualitatively very similar, indicating that the two requirements above are general and robust.

The zonally averaged model parameterizes the streamfunction associated with adiabatic buoyancy fluxes as downgradient diffusion of buoyancy thickness, with a diffusivity in the semienclosed region of the Northern Hemisphere much larger than that in the ACC region. In the simple model, the disparity in diffusivities is necessary to obtain a substantial pole-to-pole ROC. The simple model also illustrates how the geometry of the isopycnals is shaped by the interhemispheric ROC, leading to three major thermostads, which the authors identify with the major water masses of the Atlantic: that is, North Atlantic Deep Water, Antarctic Intermediate Water, and Antarctic Bottom Water.

1. Introduction

The meridional overturning circulation (MOC) is a planetary-scale pattern of oceanic flows, which is partially responsible for about 1.3 PW (1 PW = 10^{15} W) of heat transport into the North Atlantic (Ganachaud and Wunsch 2000). Changes in the North Atlantic climate have been accompanied by changes in the MOC (McManus et al. 2004; Liu et al. 2009). The MOC is also responsible for the downwelling and upwelling that regulates the uptake of CO_2 into the ocean. In particular, because the upwelling branch of the MOC is found in the Antarctic Circumpolar Current (ACC) region, changes in the winds over this region have been implicated in the deglacial warming through the release into the atmosphere of CO_2 stored in the deep ocean (Anderson et al. 2009).

Most of the poleward heat transport in the Northern Hemisphere (NH) occurs in the Atlantic sector, despite the greater extent of the Pacific Ocean (Trenberth and Caron 2001). In the Atlantic, there is a substantial heat-transporting cell with downwelling in the Northern Seas and upwelling in the ACC region (Sloyan and Rintoul 2001). In the Pacific, there is a weaker and shallower cell, which is confined to the Northern Hemisphere (MacDonald et al. 2009). In this study, we rationalize the difference between the Atlantic and the Pacific.

A schematic of the present-day overturning circulation in the Atlantic is summarized in Fig. 1, which represents the zonally averaged residual overturning circulation (ROC): that is, the sum of the Eulerian and eddy-induced flow. We focus on the ROC, rather than the MOC, because the ROC is representative of the transport of tracers such as heat. The MOC represents the volume transport and as such is not as important in the context of climate. The main contribution to the ROC comes from a pole-to-pole cell with sinking in high latitudes in the North Atlantic and upwelling in the ACC region (Lumpkin

Corresponding author address: Christopher L. Wolfe, Scripps Institution of Oceanography, University of California, San Diego, 9500 Gilman Ave., Mail Code 0213, La Jolla, CA 92093-0213.
E-mail: clwolfe@ucsd.edu
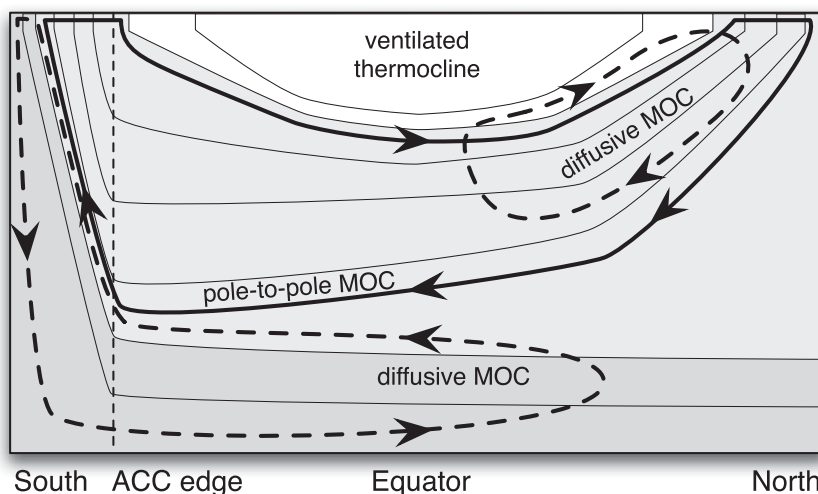
FIG. 1. A sketch of the present-day ROC as represented by the residual flow. A pole-to-pole cell (thick solid line) with sinking in high latitudes in the North Atlantic and upwelling in the ACC region coexists with weaker diffusive cells characterized by high-latitude sinking in each hemisphere and upwelling mostly confined to the same hemisphere (thick dashed lines). The thin solid lines show isopycnals. The isopycnals in the ventilated thermocline region do not outcrop in the ACC region. The isopycnals in the heavily shaded region outcrop in the channel but not in the North Atlantic. The group of three intermediate isopycnals outcrop both in the ACC and the North Atlantic, and it is along these surfaces that the pole-to-pole ROC can exist with diapycnal diffusion confined to the mixed layer. The total ROC is the combination of the pole-to-pole cell and the two diffusive cells.

and Speer 2007).[1] Interestingly, the pole-to-pole cell is such that downwelling occurs in the North Atlantic, where the surface buoyancy is actually higher than in the ACC region, where upwelling takes place. Clearly this cell cannot be buoyancy driven in the usual sense, because it flows against the buoyancy gradient.

Because of the reentrant geometry of the ACC, water exported northward in the Ekman layer can only be replaced by deep water: that is, by North Atlantic Deep Water (NADW). In this way, the NADW formed in the Northern Hemisphere can be brought to the surface by the mechanical action of the wind and transformed into light water near the surface, where diabatic mixing is plentiful (Toggweiler and Samuels 1998). This is the ''pulling'' of the ROC by the winds in the ACC (Visbeck 2007). In this sense, the driving force for this pole-to-pole cell is the wind in the ACC region. Not all of the Ekman suction results in a net formation rate: our own eddy-resolving computations indicate that only half of the Ekman transport results in water mass transformation

because of partial cancellation by eddy-buoyancy fluxes (Wolfe and Cessi 2010).

The pole-to-pole cell is augmented in the Northern Hemisphere by a weak cell with sinking in the high latitudes of the North Atlantic and North Pacific and diffuse upwelling in the tropics and subtropics (Talley et al. 2003). There is no counterpart to such a cell in the Southern Hemisphere. Instead, below the pole-to-pole cell lies a counterrotating cell with sinking in the highest latitudes of the Southern Hemisphere and diffusive upwelling in the deep ocean. These two cells are driven by diffusive upwelling, which balances high-latitude sinking (Stommel and Arons 1959; Munk and Wunsch 1998). Both diffusive cells are ''thermally direct''; that is, their flow is in the sense of reducing the equator-to-pole buoyancy gradient, consistent with the hypothesis that they are density driven. The pole-to-pole cell is thermally direct in the Northern Hemisphere but thermally indirect in the Southern Hemisphere, as noted earlier, and thus cannot be buoyancy driven.

Through a series of idealized but highly resolved computations, Wolfe and Cessi (2010) have shown that, for a substantial pole-to-pole overturning circulation to exist, two elements are required:

(i) Westerlies must drive a thermally indirect meridional flow in a reentrant high-latitude region (the

---

[1] In the zonally averaged picture, the only portion of the domain that is truly reentrant is across the latitudes of Drake Passage. A more careful treatment should follow the streamwise excursion of buoyancy surfaces into the Southern Ocean.

ACC). This configuration establishes deep stratification through the wind-driven overturning of buoyancy surfaces (the ''Deacon cell'' of the ACC), opposed by isopycnal flattening because of eddy fluxes. In the ACC region, the mechanical forcing of the wind provides the energy to bring dense fluid upward, and the reentrant geometry confines the restratifying processes to mesoscale eddies (i.e., gyres are not possible).

(ii) The meridional circulation in the ACC region must be connected to the northern sinking branch of the ROC along buoyancy surfaces that outcrop in both hemispheres, with little or no interior diapycnal mixing. Thus, the ROC only needs strong diapycnal mixing near the surface (e.g., in the mixed layer, where the circulation is closed).

The second element above implies that the strength of the overturning increases as the range of surface buoyancy values shared between the ACC region and the NH increases: that is, as the pole-to-pole difference in surface buoyancy decreases. This view is opposite to the hypothesis that the strength of the overturning increases with the pole-to-pole difference in buoyancy, as required by the classical box model of Rooth (1982). In Rooth's model (as in Stommel 1961), the energy driving the flow is supplied by the mixing implicit in the assumption that the boxes are vertically homogenous: when buoyancy differences are only applied at the surface, a buoyancy-driven circulation needs mixing to drive the buoyant fluid downward (Paparella and Young 2002). This is why we label the buoyancy-driven cells in Fig. 1 (dashed line) as diffusive. As discussed in detail in Kuhlbrodt et al. (2007), the overturning circulation in many ocean general circulation models is in the diffusive regime. Although we acknowledge that there is a diffusive component to the ROC, the focus of our work is on the quasi-adiabatic pole-to-pole ROC, driven by the winds in the ACC region.

2. Eddy-resolving computations

The quasi-adiabatic pole-to-pole ROC regime above has been illustrated in a series of idealized but highly resolved and well equilibrated computations by Wolfe and Cessi (2010). We have used the Massachusetts Institute of Technology general circulation model (MITgcm) to solve the hydrostatic primitive equations with density linearly proportional to temperature only (i.e., without salt), forced by surface temperature gradients and wind stress in a single, two-hemisphere, semienclosed basin with a reentrant channel in the southernmost eighth of the domain (see Fig. 2). Our domain is 2400 km wide, 9600 km long, and 2400 m deep (i.e., half as wide, half as long, and half as deep as the Atlantic), with a horizontal
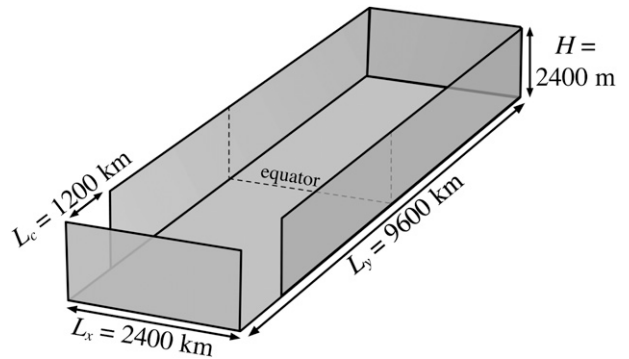
FIG. 2. The basin geometry of the numerical experiments. The horizontal resolution of the eddy-resolving and coarse-resolution models is 5.4 and 98 km, respectively. Both models use 20 unequally spaced vertical levels.

resolution of 5.4 km. There are 20 unequally spaced levels in the vertical giving a total of $1792 \times 448 \times 20$ grid points. The wind stress τ is symmetric about the equator, and the surface buoyancy is relaxed to a specified asymmetric buoyancy b^*. Each computation is run for about 300 yr, using an equilibrated run with similar parameter values as an initial condition. Because the density depends on temperature only and there is no ice, we do not have the potential for multiple equilibria, so the initial condition does not affect the final statistical equilibrium. We find that at this resolution and for a domain this size 300 yr are sufficient to reach statistical equilibrium: the equilibrium is checked by evaluating the time-averaged heat budget over the last 15 yr of the computation and requiring that the tendency term is small compared to the next largest term at each vertical level (cf. Wolfe et al. 2008).

As a measure of the buoyancy transport, we diagnose the ROC defined as

$$\psi(y,b) = -\frac{1}{T}\int_0^T dt \int_0^{L_x} dx \int_{-H}^{\zeta(x,y,b,t)} v(x,y,z,t)\,dz. \quad (1)$$

In our notation, v is the meridional velocity and $b \equiv -g(\rho/\rho_0 - 1)$ is the buoyancy, where g is the gravitational acceleration, $\rho(x, y, z, t)$ is the water density, and ρ_0 is the constant value used in the Boussinesq approximation (Vallis 2006, section 2.4). The height of the buoyancy surface b at the given position (x, y) and time t is denoted by $\zeta(x,y,b,t)$. The positions of the western and eastern boundaries are given by $x = 0$ and $x = L_x$, respectively (cf. Fig. 2), and T is the temporal averaging period. Further details on how to compute ψ are given in Wolfe and Cessi (2010).

Figure 3 shows the zonally averaged buoyancy and the ROC for three computations where the geometry or the
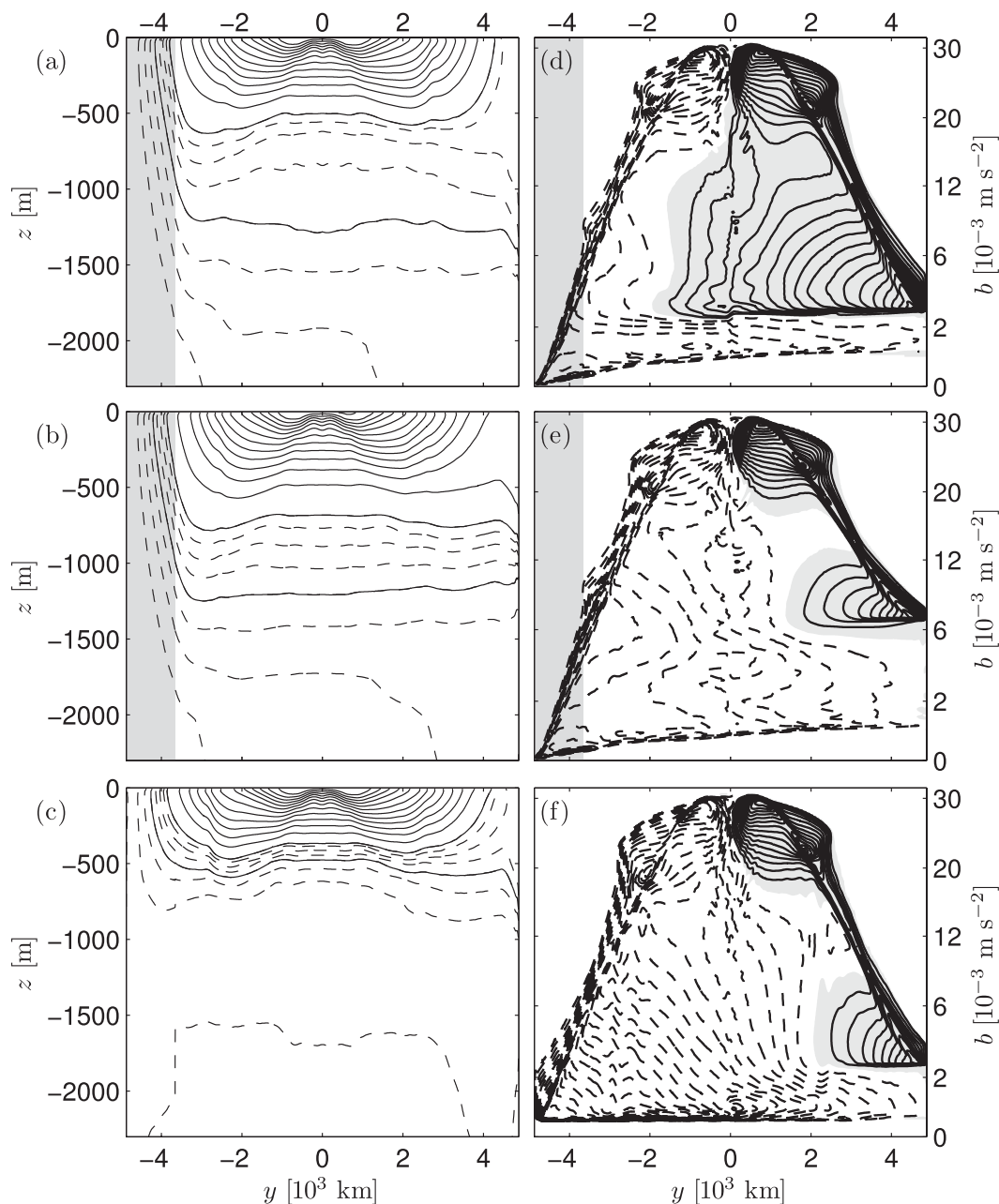
FIG. 3. (a) The zonal- and time-averaged buoyancy as a function of y and z for the control and (d) the ROC as a function of y and b for the control. The reentrant channel is shaded. Note the strong pole-to-pole ROC and the strong deep stratification. (b),(e) All parameters are identical to the control, but the surface buoyancy in the NH is increased so that there are no shared outcropping values between the NH and the channel. (e),(f) All parameters are identical to the control, but the channel is closed. The contour intervals for (a)–(c) are 2×10^{-3} m s^{-2} (solid) and 5×10^{-4} m s^{-2} (dashed). The contour interval for (d)–(f) is 0.5 Sv. Positive values are solid, negative values are dashed, and the area of positive contours is shaded.

relaxation surface buoyancy is varied. For all computations, the diapycnal diffusivity is constant and given by $\kappa_v = 5 \times 10^{-5}$ m^2 s^{-1} (there is also convective adjustment). Other values of the parameters are given in Wolfe and Cessi (2010).

The forcings, given in Wolfe and Cessi (2010), are

$$\tau = \tau_0 \left[-\cos\frac{3\pi y}{2L_y} + 0.8 e^{-(y/L_y)^2/0.016} \right] \quad \text{and} \quad (2)$$

$$b^* = b_e \left[1 + \cos\frac{\pi y}{L_y} - \epsilon \left(1 + \sin\frac{\pi y}{2L_y} \right) + \Delta e^{-(y/L_y - 1)^2/16} \right],$$
(3)

where τ_0 and b_e are the amplitudes of the wind and buoyancy forcing, respectively; ϵ measures the small asymmetry between the surface buoyancy in the Southern and Northern Hemispheres; and Δ controls whether there are shared surface buoyancy values between the ACC region and the high-latitude Northern Hemisphere. For all computations in Fig. 3, we use the following values of the parameters:

$$L_y = 4.88 \times 10^6 \, \text{m}, \quad \tau_0 = 0.1 \, \text{N m}^{-2},$$
(4)

$$b_e = 0.0152 \, \text{m s}^{-2}, \quad \text{and} \quad \epsilon = -0.081.$$
(5)

In Figs. 3a,d, the forcing is such that the northernmost surface buoyancy value is also found at the surface in the reentrant region, as is the case for the current climate configuration in the Atlantic sector. This arrangement is obtained by setting $\Delta = 0$ in (3). For $\Delta = 0.27$ (Figs. 3b,e), there are no surface buoyancy values shared between the reentrant region and the Northern Hemisphere. This is the current climate configuration in the Pacific sector. In this case, even though the equator-to-pole buoyancy gradient in the Northern Hemisphere is reduced by a mere 15%, the ROC is much weaker (Fig. 3e), because a pole-to-pole circulation with an adiabatic interior cannot be established and the residual circulation is necessarily diffusive. However, the deep and intermediate buoyancy distributions are not qualitatively changed from the control (cf. Figs. 3a,b). If the whole domain is closed (i.e., there is no reentrant region; Figs. 3c,f), the stratification below the main thermocline is much reduced compared to the control, as is the residual transport. This is because gyres can be supported by east–west pressure differences in a domain with side boundaries. In turn, gyres return the Ekman transport at a shallow level, unlike the deep overturning Deacon cell obtained in the reentrant geometry, which goes all the way to the bottom of the reentrant portion of the domain. Another way of contrasting the circulation in a blocked versus reentrant geometry is to consider that gyres are more efficient than mesoscale eddies at flattening isopycnals, so the resulting intermediate and deep stratification is much weaker in the blocked case.

Our computations show that increasing the range of surface buoyancies in common between the ACC and that the high-latitude Northern Hemisphere strengthens the pole-to-pole component of the ROC. Either decreasing the buoyancy in the North Atlantic or increasing the
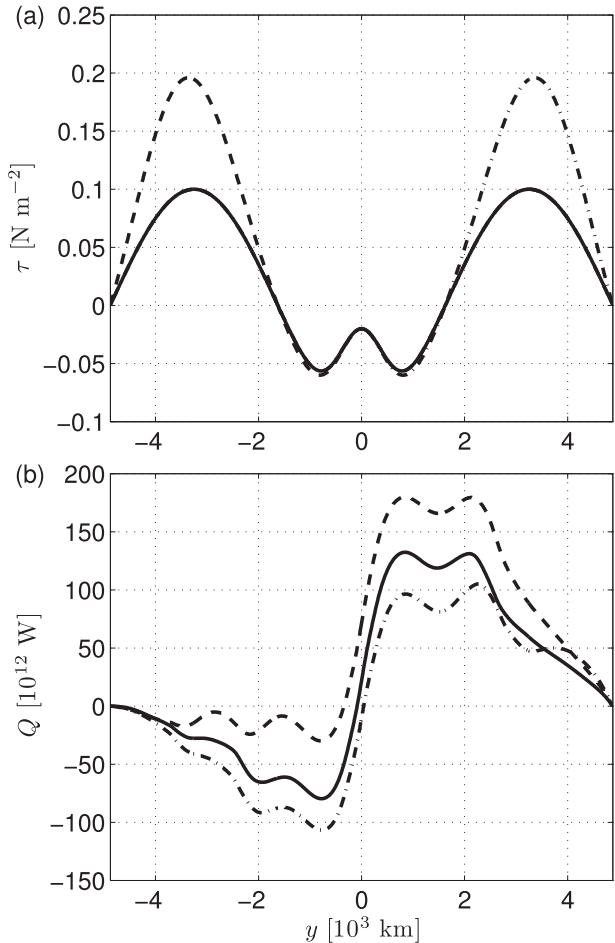
FIG. 4. (a) Zonal wind stress τ and (b) meridional heat transport Q for the control (solid), increased southern wind (dashed), and increased northern wind (dashed–dotted) experiments.

buoyancy in the ACC, widens the "window" of shared surface densities, and, as will be shown in the next section, this results in a stronger ROC.

Implicit evidence that the "shared buoyancy" mechanism is operative has been provided before. In particular, it has been shown that increasing the buoyancy in the ACC region strengthens the North Atlantic MOC (Knorr and Lohmann 2003; Weaver et al. 2003). Our computations demonstrate that there is "threshold" behavior: unless there are shared buoyancy values between the Northern Hemisphere and the ACC region, no pole-to-pole quasi-adiabatic circulation can be established and only the weak diffusive cells can be supported.

Another way to control the strength of the pole-to-pole ROC is to change the wind forcing over the subpolar regions. Figure 4 shows the results of two experiments in which the wind stress is increased by a factor of 2 (Fig. 4a) over either the northern (dashed–dotted) or southern (dashed) subpolar region. Because the ROC is

"pulled" from the south and "pushed" from the north, the two wind perturbations have opposite effects: the ROC is strengthened by increased wind stress in the Southern Hemisphere and weakened by increased wind stress in the Northern Hemisphere. These changes are reflected in the meridional heat transport: in the experiment with increased southern winds, the strengthened ROC transports an additional 50×10^{12} W into the Northern Hemisphere (dashed line in Fig. 4b), resulting in cooler water in the southern subpolar region and warmer water in the northern subpolar region. Increasing the wind in the Northern Hemisphere has the opposite effect: the meridional heat transport is reduced by 30×10^{12} W (dashed–dotted line in Fig. 4b), leading to cooling in the north and warming in the south.[2]

3. The adiabatic limit in a coarse-resolution model

The eddy-resolving computations are very demanding and do not allow extensive experimentation with changes in the value of the parameters. In particular, as the vertical diffusivity is decreased, the computations become more formidable because the abyss takes an increasing longer time to equilibrate. Therefore, to explore a more adiabatic regime, we resort to a three-dimensional coarse-resolution model where the mesoscale eddies are parameterized using the boundary value method of Ferrari et al. (2010) with constant eddy diffusivity $\kappa = 488$ m^2 s^{-1}. The geometry (cf. Fig. 2) and the shape of the forcings [cf. Eqs. (2) and (3)] are the same as the eddy-resolving computations of section 2, but, because of the coarser resolution (98 km in the horizontal direction), the lateral viscosity is a factor of 1000 larger than in the eddy-resolving computations. We consider the limit where the buoyancy diffusivity is zero, except in a mixed layer, where the vertical diffusion is given by

$$\kappa_v = \kappa_s e^{-z^2/(2d_s^2)}, \qquad (6)$$

with $d_s = 40$ m and $\kappa_s = 5.3 \times 10^{-3}$ m^2 s^{-1}. Horizontal diffusivity in the mixed layer is provided by the Redi (1982) isopycnal mixing scheme, which is tapered exponentially to horizontal diffusion with diffusivity $\kappa_I = 488$ m^2 s^{-1} when the isopycnal slope is greater than $\frac{1}{250}$, using the tapering scheme of Danabasoglu and McWilliams (1995). Note that the isopycnal component of the Redi scheme has no effect in the interior because of the use of a single component equation of state. There is also diapycnal diffusivity

due to convective adjustment and a small amount of numerical diffusion due to the flux-limiting advection scheme [a multidimensional implementation of the one-step, seventh-order, monotonicity-preserving scheme of Daru and Tenaud (2003)].

Figure 5 shows the zonally and temporally averaged buoyancy and the ROC, using the same geometry and forcings of the eddy-resolving computations. The intermediate stratification is similar to the eddy-resolving runs (Figs. 3a–c), but the vertical gradients of b are stronger because of the reduced interior diffusivity. The diffusive components of the ROC are significantly reduced compared to the eddy-resolving runs, and thus the pole-to-pole component of the ROC is more clearly distinguished: this is the shaded set of contours in Fig. 5d. The diffusive cells (the positive contours in the high latitudes of the Northern Hemisphere) are of comparable magnitude regardless of the geometry of the calculations and occupy the same region in b space (cf. Figs. 5e,f); however, in physical space, the diffusive component of the ROC is much shallower in the closed geometry.

When the forcing is such that there is a range of surface buoyancy values shared between the Northern Hemisphere and the channel (Figs. 5a,d), a thermostad dividing the shared and unshared outcropping buoyancy contours becomes apparent: this is region in which the pole-to-pole ROC travels southward. In this calculation, the pole-to-pole ROC peaks at approximately 1 Sv (1 Sv $\equiv$ 10^6 m^3 s^{-1}) and extends well into the ACC region. Figures 5b,e show the case where $\Delta = 0.27$ in (3): that is, when there are no outcropping buoyancy values shared between the Northern Hemisphere and the channel. In agreement with the eddy-resolving calculations, the middepth thermostad and pole-to-pole component of the ROC collapse, but the intermediate stratification is similar to that shown Fig. 5a. If the reentrant region is removed (Figs. 5c,f), the water beneath the main thermocline is nearly homogeneous and the ROC is weak.

To further illustrate the importance of the shared surface buoyancy window, we performed an additional calculation with

$$b^* = b_e \left[1 + \cos\frac{\pi y}{L_y} - \epsilon \left(1 + \sin\frac{\pi y}{2L_y} \right) + \Delta e^{-(y/L_y+1)^2/16} \right], \qquad (7)$$

with $\Delta = -0.27$ and all the other parameters are as in (4) and (5). In this case, the forcing has a negative buoyancy perturbation at the southern end of the domain rather than a positive one at the northern end, as in Figs. 5b,e. There is thus no pole-to-pole window of shared surface buoyancy because all the surface buoyancy values in the

---

[2] For this computation, we did not save the time series of b and v necessary to diagnose the ROC, and this is why the meridional heat transport, rather than the ROC, is shown.
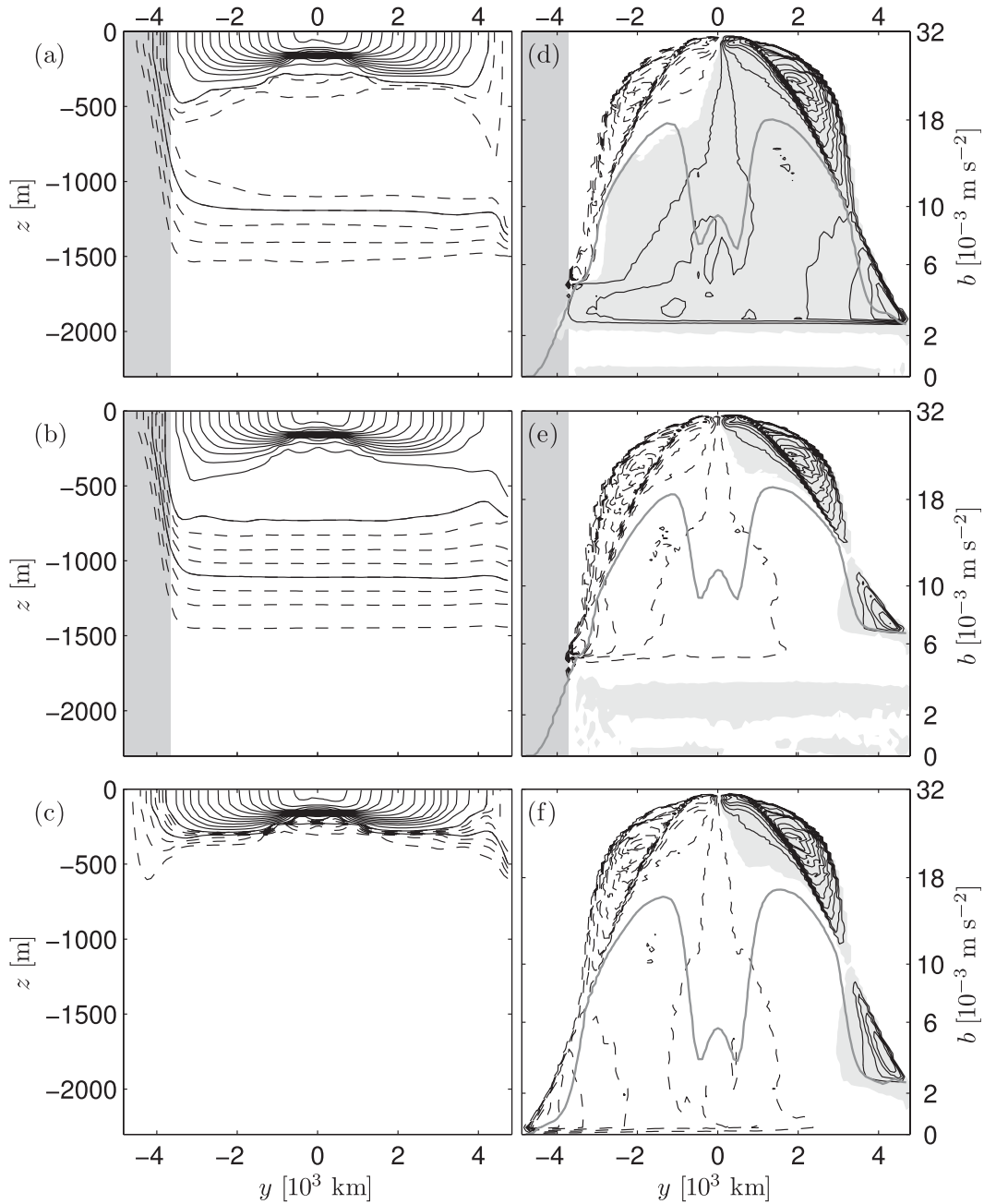
FIG. 5. As in Fig. 3, but for the coarse-resolution model. The contour intervals are as in Fig. 3. The thick gray line gives the position of the base of the mixed layer in buoyancy coordinates.

ACC are smaller than those in the Northern Hemisphere. Figures 6a,b show the zonally and temporally averaged buoyancy and the ROC, respectively: because the range of buoyancies is increased, the stratification is stronger. However, even though the pole-to-pole buoyancy difference is increased and the equator-to-pole difference in the Northern Hemisphere is the same as that of Fig. 5d, the ROC is weak and comparable to that in Fig. 5e. Thus the ROC can be decreased to the Pacific

configuration of Fig. 5d by either increasing the buoyancy at the northern end of the domain (Fig. 5e) or decreasing the buoyancy at the southern end of the domain (Fig. 6). Both cases demonstrate the necessity of a window of surface buoyancy values shared between the ACC and the Northern Hemisphere.

Because the residual circulation ultimately needs diabatic processes, one might assume that the ROC obtained in Fig. 5d depends on the magnitude of the mixed layer
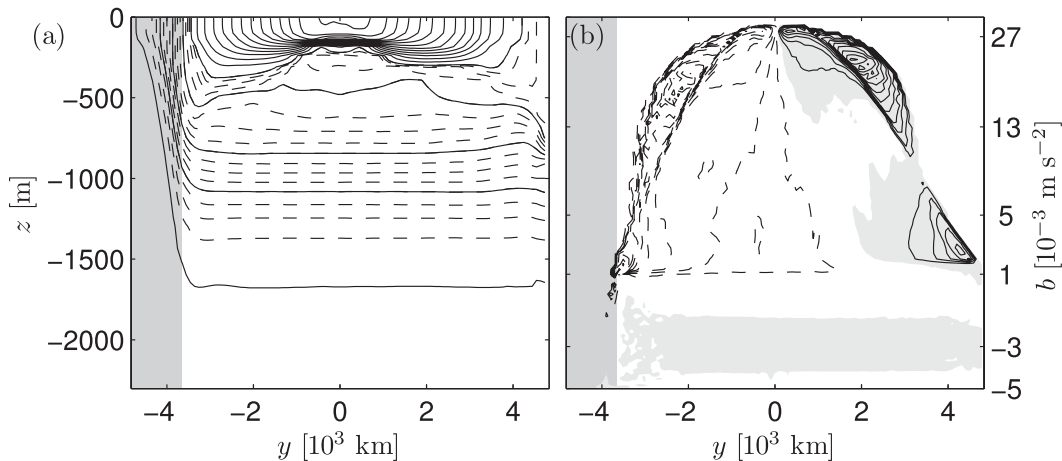
FIG. 6. As in Fig. 5 (top) except that the surface buoyancy forcing is given by (7). The contour intervals are as in Fig. 5.

diapycnal diffusivity. However, we term the pole-to-pole ROC quasi adiabatic, because for sufficient mixed layer diffusion (and small enough interior diffusivity) the ROC becomes independent of the diffusivity. To test this hypothesis, we performed another calculation, with the same parameters as those used for Figs. 5a,d, except that the mixed layer diffusivity is doubled and it gives the same stratification and ROC (not shown).

To make progress in understanding how the pole-to-pole circulation is established, we partition the zonally averaged ROC ψ into two components: the MOC $\overline{\psi}$, which is the streamfunction for the zonally and temporally averaged meridional velocity $\overline{v}$, and the eddy streamfunction ψ^e, which is associated with the meridional buoyancy transport due to flows with zero time and zonal mean v' (i.e., eddies and gyres).[3] Specifically, we define

$$\overline{v}(y,z) \equiv \frac{1}{L_x}\int_0^{L_x} dx \, \frac{1}{T}\int_0^T dt \, v \quad \text{and} \quad v'(x,y,z,t) \equiv v - \overline{v}.$$ (8)

The corresponding streamfunctions are given by

$$\overline{\psi} \equiv -\int_{-H}^z \overline{v}(y,\tilde{z}) \, d\tilde{z} \quad \text{and} \quad \psi^e \equiv \psi - \overline{\psi},$$ (9)

where the overbar indicates time and zonal averaging and ψ is defined in (1).

---

[3] The gyral circulation is three dimensional and thus also has a zonally averaged component associated with the return of the Ekman flow, which occurs primarily in the western boundary. This part of the gyral circulation is included in $\overline{\psi}$, whereas the purely horizontal circulation is in ψ^e.

Figure 7 shows $\overline{\psi}$ and ψ^e for the computation in Figs. 5a,d. Figure 7a shows $\overline{\psi}$ as a function of y and b as well as the mean isopycnal height $\overline{z}$, which is defined by

$$\overline{z}(y,b) = -H + \frac{1}{T}\int_0^T dt \, \frac{1}{L_x}\int_0^{L_x} dx \, \zeta(x,y,b,t). \quad (10)$$

The Ekman cells occupy the upper part of the buoyancy values and, correspondingly, the shallower part of the water column, except in the reentrant region, where the Deacon cell fills the whole depth of the domain. The Deacon cell tends to overturn the isopycnals in a clockwise direction because the Ekman flow $\overline{\tau}/f$ is negative in this region. Because in the ACC there is no $\overline{v}$ between the thin top and bottom Ekman layers, the streamlines of the Deacon cell are independent of b (or z) in the interior. In the enclosed portion of the domain, the return flow of the Ekman transport is affected by the gyral circulation and occurs within the thermocline.

In addition to the Ekman cells, Fig. 7a shows a deep meridional overturning cell with flow down the mean isopycnal thickness gradient. This flow is the buoyancy-coordinate analog of frictional flow down the meridional buoyancy gradient which often parameterizes the meridional overturning circulation in zonally averaged models (Marotzke et al. 1988; Wright and Stocker 1991; Marchal et al. 2007). This component of the overturning circulation is in geostrophic balance with a large-scale buoyancy difference between the eastern and western boundaries (cf. Cessi and Wolfe 2009).

The sum of Figs. 7b,c gives ψ^e, and we further partition this component into a contribution due to the gyres and a component due to the Gent–McWilliams subgrid parameterization of mesoscale eddies. The latter component (Fig. 7c) is only important in the reentrant portion of

the domain, where it almost completely cancels the Deacon cell. The component of ψ^e due to the gyres (Fig. 7b) exists only in the enclosed region. It is systematically in the opposite direction of $\overline{\psi}$ and is larger than the eddy component shown in Fig. 6c: in the region of westerlies, the gyral part of ψ^e reverses the sense of circulation of the Ekman return flow, something the eddies fail to accomplish.

4. A conceptual model of the adiabatic ROC

In this section, we develop an idealized model of the ROC that accounts for its various components, emphasizing the differences in dynamics between the reentrant and enclosed portions of the domain. We frame our development in terms of the zonally averaged diagnostics presented in the previous section.

The temporally and zonally averaged buoyancy equation reads

$$\partial_y(\overline{\psi}\overline{b}_z + \overline{v'b'}) - \partial_z(\overline{\psi}\overline{b}_y - \overline{w'b'}) = \partial_z\overline{F}, \quad (11)$$

where $\overline{b}_y = \partial_y\overline{b}$, $\overline{b}_z = \partial_z\overline{b}$, and $\overline{F}$ is the diabatic vertical flux of buoyancy. We can associate the eddy streamfunction ψ^e with

$$\psi^e = \frac{\overline{v'b'}}{\overline{b}_z}. \quad (12)$$

Other definitions of ψ^e are possible that avoid the singularity when $\overline{b}_z = 0$ (cf. Plumb and Ferrari 2005), but this is not necessary for the development that follows. With $\psi = \overline{\psi} + \psi^e$, we can rewrite (11) as

$$\partial_y(\psi\overline{b}_z) - \partial_z(\psi\overline{b}_y) = \partial_z\overline{F} - \partial_z\left(\frac{\overline{v'b'}\,\overline{b}_y + \overline{w'b'}\,\overline{b}_z}{\overline{b}_z}\right). \quad (13)$$

We have rearranged terms to emphasize that the last term on the right-hand side represents the diapycnal eddy flux and is thus part of the diabatic forcing. We have denoted with ψ the residual streamfunction: with the definition (12), the residual is an approximation to (1), accurate in the limit of small buoyancy variance.

FIG. 7. (a) The zonally averaged component of the ROC shown in Fig. 5d, where the zonal average is performed at fixed z levels as a function of y and b. (c) The portion of the transport due to the modified Gent–McWilliams parameterization and (b) the remainder, which is associated with flows with zero zonal average that are resolved by the computation (i.e., gyres, large-scale waves, and eddies). The contour intervals are as in Figs. 5d–f. The mean isopycnal height field is additionally contoured using thin gray lines; the contour interval is 100 m.

We assume that the idealized dynamics of the intermediate/deep circulation has two distinct regimes: a diabatic mixed layer in the surface region where $-d \leq z \leq 0$ and an adiabatic interior in the rest of the domain. In the mixed layer, diabatic effects are important and buoyancy is independent of depth to a first approximation. In other words, in the mixed layer, buoyancy is governed by (Marshall and Radko 2003; Radko 2007)

$$-\partial_z \psi \overline{b}_y \approx \partial_z \overline{F}. \qquad (14)$$

For simplicity, we neglect the effect of diabatic eddies in the mixed layer, although they could be included if suitably parameterized.[4] Because $\overline{b}$ is independent of z in the mixed layer, (14) can be integrated over the depth of the mixed layer d. At the surface, the ROC must vanish and the buoyancy is relaxed to a prescribed surface buoyancy distribution b^* at the rate w^*/d; that is, the boundary conditions at $z = 0$ are

$$\psi = 0 \quad \text{and} \quad \overline{F} = w^*(\overline{b}^* - \overline{b}). \qquad (15)$$

At the bottom of the mixed layer, we assume that diabatic effects vanish so $\overline{F} = 0$ at $z = -d$. Then, the residual streamfunction at the bottom of the mixed layer satisfies

$$\psi \frac{d\overline{b}}{dy} = w^*(\overline{b}^* - \overline{b}). \qquad (16)$$

In the adiabatic interior, we neglect all sources of diapycnal forcing, so the ROC obeys

$$\partial_y \psi \overline{b}_z - \partial_z \psi \overline{b}_y = 0, \qquad (17)$$

whose general solution is

$$\psi = \psi(\overline{b}). \qquad (18)$$

In other words, within the adiabatic region, contours of constant ψ coincide with contours of constant $\overline{b}$. For those buoyancy contours that intersect a solid boundary, $\psi = 0$. A nonzero adiabatic ROC can only exist along those buoyancy surfaces that intersect the mixed layer (and thus the surface) at least twice, as shown in Fig. 1. The circulation thus established is closed in the mixed layer. The functional form between ψ and $\overline{b}$ is determined by requiring continuity of ψ at the bottom of the mixed

layer. In other words, we rewrite (16) in buoyancy coordinates; that is,

$$\psi(\overline{b}) = \frac{dy_s}{d\overline{b}} w^* [\overline{b}^*(y_s) - \overline{b}], \qquad (19)$$

where $y_s(\overline{b})$ is the outcrop latitude of $\overline{b}$ in the Southern Hemisphere. It must also be the case that

$$\psi(\overline{b}) = \frac{dy_n}{d\overline{b}} w^* [\overline{b}^*(y_n) - \overline{b}], \qquad (20)$$

where $y_n(\overline{b})$ is the outcrop latitude of $\overline{b}$ in the Northern Hemisphere. A third equation is needed to determine the unknowns ψ, y_s, and y_n, and this comes from the prescription of the mean and eddy buoyancy transports $\overline{\psi}$ and ψ^e as a function of y and z (or y and $\overline{b}$) in the interior region.

In the reentrant region, $-L_y \leq y \leq -3L_y/4$, $\overline{v} = 0$, and the mean and eddy streamfunctions are given by (Karsten et al. 2002)

$$\overline{\psi}_{ACC} = -\frac{1}{f} \frac{\tau}{\rho} \quad \text{and} \quad \psi^e_{ACC} = -\kappa_A \frac{\overline{b}_y}{\overline{b}_z}, \qquad (21)$$

where $\overline{\tau}$ is the zonally averaged east–west wind stress and $f = \beta y$ is the Coriolis parameter. In the ACC region, the Ekman transport, which we assume occurs in the mixed layer region above $z = -d$, is returned at the bottom of the reentrant region (or below it, if there is a sill). Thus, in the interior region, $\overline{\psi}$ is independent of z; $\overline{v} = 0$; and $\overline{w}$, equal to the Ekman suction, goes all the way to the bottom. The eddy diffusivity κ_A has a value appropriate for mesoscale eddies, because this is the only type of structure that can contribute to $\overline{v'b'}$ in the ACC region.

In the enclosed portion of the basin, several components of the flow contribute to $\overline{v}$ below the mixed layer, including a geostrophic one, because an east–west pressure difference can be supported by the solid boundaries. This pressure difference balances the return flow of the surface Ekman transport, which, in a stratified ocean, decays with depth and occurs mostly within the wind-driven thermocline (cf. the upper cells shown in Fig. 7b). In addition to the Ekman return flow, there is a deep meridional overturning cell with flow down the gradient of mean isopycnal height, described in section 2. This cell is in geostrophic balance with a large-scale buoyancy difference between the eastern and western boundaries.

Further buoyancy transport is affected by the horizontal flow in the gyres, which, although it has no zonally averaged velocity, carries buoyancy meridionally more effectively than mesoscale eddies (cf. Fig. 7c). Thus, for those buoyancy contours outcropping in both the ACC

---

[4] When comparing the results to the coarse-resolution model, this neglect of mixed layer eddies is entirely justified: the time scale associated with parameterized eddy mixing on the basin scale $t_D = L_x^2/\kappa \approx 10^9$ s is much longer than the surface relaxation time scale $t_R = d/w^* \approx 10^6$ s.

and the Northern Hemisphere, we parameterize the complex three-dimensional residual circulation in the enclosed portion of the basin as

$$\psi_{\text{basin}} = -\frac{f}{f^2 + r^2}\frac{\overline{\tau}}{\rho}e^{\alpha(\overline{b}-\overline{b}_0)} - \kappa_{\text{B}}\frac{\overline{b}_y}{\overline{b}_z}. \quad (22)$$

There are two differences between the residual streamfunctions in the reentrant and enclosed parts of the basin: 1) the return flow of the Ekman transport occurs at a shallow level in the enclosed region and this is parameterized as a decay from the surface buoyancy, $b = b_0$, over the buoyancy scale α^{-1} (we also add some small distributed friction r to cure the singularity of the Ekman transport at the equator); 2) in the enclosed region, a zonally averaged flow down the mean buoyancy gradient is allowed, in addition to the buoyancy transport effected by eddies and gyres with no zonal mean. The aggregate of these flows is parameterized to be proportional to the gradient of the buoyancy surface's height, in analogy with the Gent–McWilliams parameterization (Gent et al. 1995), but with a diffusivity κ_{B} much larger than that appropriate for mesoscale eddies κ_{A}.

A parameterization of the zonally averaged buoyancy-driven component of the ROC in terms of the buoyancy slope cannot be rigorously justified. Usually, the zonally averaged transport is taken proportional to the zonally averaged buoyancy gradient (Marotzke et al. 1988; Wright and Stocker 1991; Marchal et al. 2007). Instead, we parameterize the ROC as having a component proportional to the gradient of the isopycnal height (i.e., down the buoyancy slope), which is the natural choice when working in buoyancy coordinates. This form is neither more[5] nor less justifiable than previously adopted parameterizations, and it is amenable to analysis when working in buoyancy coordinates. Further, this parameterization is consistent with the observation in section 3 of a deep overturning cell, which flows down the meridional gradient of mean isopycnal height (cf. Fig. 7a). For those buoyancy contours that surface only in the ACC region, we assume that $\psi = 0$ in the enclosed portion of the basin, because these contours encounter the solid boundary in the Northern Hemisphere.

It is useful to rewrite (21) and (22) in buoyancy coordinates, using the definition

$$\frac{\partial \overline{z}(y,\overline{b})}{\partial y} = -\frac{\overline{b}_y}{\overline{b}_z}, \quad (23)$$

where $\overline{z}$ is the mean depth of the isopycnal $\overline{b}$, which is defined in (10). We can then unify (21) and (22) into the single formulation,

$$\psi = -\frac{f}{f^2 + r^2}\frac{\overline{\tau}}{\rho}\phi + \kappa_e\frac{\partial \overline{z}}{\partial y}, \quad (24)$$

where

$$\phi = \begin{cases} 1 & \text{if} \quad y < -3L_y/4 \\ e^{\alpha(\overline{b}-\overline{b}_0)} & \text{if} \quad y \geq -3L_y/4 \end{cases} \quad \text{and} \quad (25)$$

$$\kappa_e = \begin{cases} \kappa_{\text{A}} & \text{if} \quad y < -3L_y/4 \\ \kappa_{\text{B}} & \text{if} \quad y \geq -3L_y/4 \end{cases}. \quad (26)$$

Because ψ depends on $\overline{b}$ only, (24) is easily integrated to give

$$\overline{z} = -d + \int_{y_s}^{y}\phi\frac{f}{f^2 + r^2}\frac{\overline{\tau}}{\kappa_e\rho}\,d\tilde{y} + \psi\int_{y_s}^{y}\frac{d\tilde{y}}{\kappa_e}, \quad (27)$$

where we have used the condition that $\overline{z} = -d$ at $y = y_s(\overline{b})$. For those isopycnals that only surface in the ACC region, $\psi = 0$, and $\overline{z}(y,\overline{b})$ is readily obtained from (27). For those isopycnals that intersect the surface again, we also need to impose $\overline{z} = -d$ at $y = y_n(\overline{b})$, and this condition determines ψ to be

$$\psi = -\left(\int_{y_s}^{y_n}\frac{dy}{\kappa_e}\right)^{-1}\int_{y_s}^{y_n}\phi\frac{f}{f^2 + r^2}\frac{\overline{\tau}}{\kappa_e\rho}\,dy. \quad (28)$$

This relation, together with (19) and (20), completes the set of equations to be solved to find $\psi(b)$, $y_s(b)$, and $y_n(b)$. Once these three quantities are determined, (27) gives $\overline{z}(y,\overline{b})$ or alternatively $\overline{b}(y,\overline{z})$. Notice that the strength of the mixed layer diffusivity does not appear anywhere. By assuming that the mixed layer has enough mixing to keep the buoyancy vertically homogeneous, the amplitude of the ROC is determined by the interior adiabatic dynamics and the surface boundary conditions. This assumption is motivated by the results of the coarse-resolution calculation (cf. section 3), which show that the final buoyancy and ROC are independent of the diffusivity.

To illustrate the solution, we solve the system (19), (20), and (28) in the limit of rapid relaxation (i.e., for $w^*L_y \gg \psi$). In this limit, the surface buoyancy is approximately clamped to the prescribed buoyancy, so that $b_0(y) \approx b^*(y)$ and the solutions of (19) and (20) are

$$y_s \approx b^{*-1}(\overline{b}) \quad \text{and} \quad y_n \approx b^{*-1}(\overline{b}). \quad (29)$$

---

[5] Gent et al. (1995) argue that this is the correct form for flows that are quasi adiabatic and decrease the available potential energy.
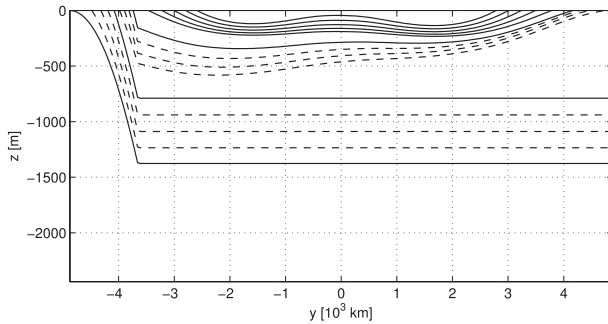
FIG. 8. The buoyancy field $\overline{b}(y, \overline{z})$ obtained as a solution to (27) with ψ given by (28). The contour interval is as in Figs. 3a–c. The solution is omitted for those contours outcropping more than twice, because the expression (28) is not valid in that case.

Using the forcing in (3) with $\Delta = 0$ and exploiting the smallness of ϵ, we have

$$y_{s,n}(\overline{b}) \approx \mp \frac{L_y}{\pi} \arccos\left[\frac{\overline{b} - b_e}{b_e} \mp \epsilon \sin\left(\frac{1}{2} \arccos\frac{\overline{b} - b_e}{b_e}\right) + \epsilon\right],$$

$$(30)$$

where the $-$ refers to y_s and the $+$ refers to y_n. Figures 8 and 9 show $\overline{b}(y, \overline{z})$, obtained from (27), and the corresponding $\psi(\overline{b})$, given by (28), respectively, using the values of the parameters given in (4) and the following additional parameters:

$$\rho = 1000 \, \text{kg m}^{-3}, \quad \beta = 2.3 \times 10^{-11} \, \text{m}^{-1} \, \text{s}^{-1}, \quad (31)$$

$$\tau = 1.4 \times 10^{-5} \, \text{s}^{-1}, \quad \alpha = 1.5 b_e^{-1}, \quad (32)$$

$$\kappa_A = 488 \, \text{m}^2 \, \text{s}^{-1}, \quad \text{and} \quad \kappa_B = 4880 \, \text{m}^2 \, \text{s}^{-1}. \quad (33)$$

The slopes of the zonally averaged isopycnals (Fig. 8) compare well with those found in both the low-resolution computations (Fig. 5a) and the eddy-resolving runs (Fig. 3a), including the reversal found in the subtropics. This qualitative agreement supports the parameterization of the buoyancy-driven component of the ROC down the isopycnals slope.

In addition, the simple model gives some insight in how the thermostads are formed. There are two kinds of buoyancy contours that outcrop in the ACC: those that also outcrop in the Northern Hemisphere and those that do not. The two sets of contours are separated by a thermostad whose thickness increases toward the north, and that we identify as North Atlantic Deep Water. Because ψ is positive for most of the shared outcropping contours (cf. Fig. 9), their slope in the ACC is less than that of the contours with $\psi = 0$ [cf. (27)]. The relative shoaling of the
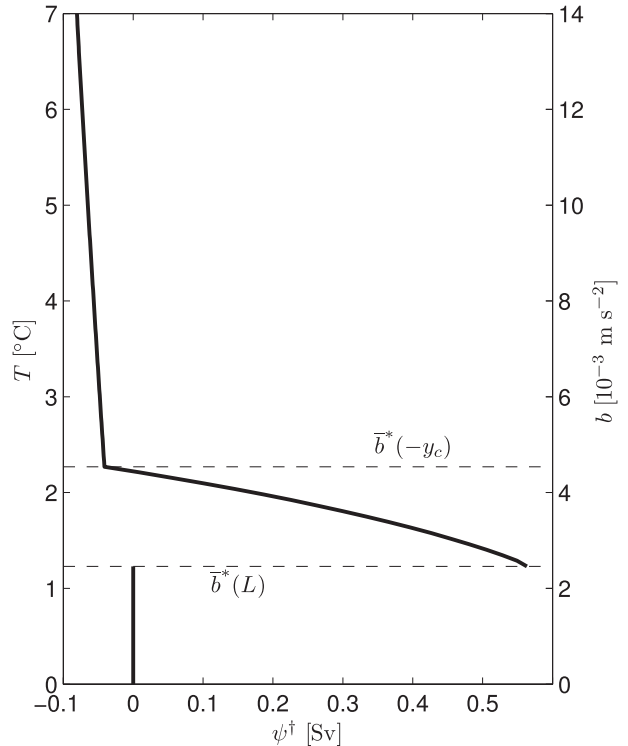
FIG. 9. ROC $\psi(b)$ corresponding the buoyancy field shown in Fig. 8. The values of the surface buoyancy profile b^* at the northern boundary, $y = L$, and the northern edge of the channel, $y = -y_c$, are indicated.

shared outcropping buoyancy contours gives rise to the thermostad in the enclosed portion of the domain. It is clear that the geometry of the shared contours depends on the dynamics of the global ocean: ψ is given by an integral of the wind stress and eddy diffusivity along all the latitudes encompassed by each isopycnal. This is not the case for the buoyancy values that do not outcrop in the Northern Hemisphere: in the ACC region, the slope of the isopycnals depends on the local wind stress and eddy transport. In the adiabatic limit, these isopycnals are flat north of the channel, and their depth is determined at the equatorial edge of the ACC region.

Similarly, there are two kinds of buoyancy contours that outcrop in the Northern Hemisphere: those that also outcrop in the ACC and those that outcrop again in the enclosed portion of the basin. The latter buoyancy surfaces have shallower slopes than the former because they are not subject to the steepening effect of the Deacon cell. The relative shoaling of the contours not outcropping in the ACC region leads to another shallow thermostad, which we identify with Antarctic Intermediate Water.

In summary, the simple conceptual model produces three thermostads: a shallow one separating buoyancy contours that outcrop twice in the enclosed portion of

the basin from those that outcrop in the Northern Hemisphere and the ACC region; an intermediate thermostad separating buoyancy contours that outcrop in the ACC and the Northern Hemisphere and buoyancy contours that only outcrop in the ACC; and a bottom thermostad comprising the densest waters outcropping in the ACC only.

Because the term proportional to the buoyancy slope in (24) is a parameterization of the three-dimensional dynamics of the gyres, boundary currents, waves, and eddies, the pole-to-pole ROC depends on the global circulation. Given that κ_e is smaller in the ACC region and it appears in the denominator inside the integrals (24) and (28), the dynamics of the ACC region contributes the most to the ROC.

Because ψ decreases monotonically with $\overline{b}$ and $\overline{b}$ is a monotonically decreasing function of $\overline{z}$, the residual meridional flow is toward the north everywhere along the shared contours. This implies that the southward return flow occurs within the North Atlantic Deep Water thermostad region, where the solution to the adiabatic buoyancy budget (17) is $\overline{b}$ = constant. This is indeed what we find in the eddy-resolving and coarse-resolution calculations (Figs. 3a,d and 5a,d). Implicitly, we assume that a diffusive boundary layer smoothes the transition between the thermostad and the region where $\overline{b}$ is not constant.

To understand the dependence of ψ on the model parameters, it is useful to examine the limit where the buoyancy forcing in (3) is symmetric around the equator: that is, when $\epsilon = 0$. In that case, because τ/f is antisymmetric across the equator, the only contribution to the integral of τ/f in the enclosed region comes from the latitudes $3L_y/4 < y < L_y$: that is, the latitudes in the Northern Hemisphere corresponding to those of the ACC region. The wind stress contribution in the remaining portion of the enclosed basin vanishes by symmetry. Then, if we further assume that $\alpha = 0$ in (25), ψ is given by

$$\psi = \left(\frac{\kappa_B}{\kappa_A} - 1\right)\left[y_n + y_c - (y_c + y_s)\frac{\kappa_B}{\kappa_A}\right]^{-1}\int_{y_c}^{y_n}\frac{\tau}{\rho f}\,dy, \quad (34)$$

where $-y_c$ denotes the equatorward edge of the reentrant region. Thus, for symmetric winds and buoyancy forcing, the ROC increases as the difference between κ_B and κ_A increases. This is consistent with the calculation by Radko (2007), who finds zero residual circulation when considering an aquaplanet with symmetric forcing across the equator.

In the limit where $\kappa_B \gg \kappa_A$, the integrals in (28) are dominated by the contribution from the ACC region, and the residual streamfunction is given by

$$\psi \approx (y_c + y_s)^{-1}\int_{y_s}^{-y_c}\frac{\overline{\tau}}{\rho f}\,dy, \quad (35)$$

so that the surface Ekman transport and buoyancy forcing in the ACC control the strength of the ROC. In this limit, the ROC becomes independent of the poorly constrained values of the eddy diffusivities. The ROC also depends on the latitudinal width of the window of shared surface buoyancies, which is here measured by the distance $y_c + y_s$.

In the limit of a window of narrow latitudinal extent, the ROC is just given by $\psi \approx \tau(y_c)/(\rho f(y_c))$, which, using values appropriate for the latitudes of Drake passage gives $\psi \approx 1$ m^2 s^{-1}. To turn this zonally averaged transport into volume transport, we need to multiply by the longitudinal extent of the surface isopycnals at Drake Passage in common with the Northern Hemisphere. Our single-ocean model does not provide useful guidance on how far this window spreads longitudinally in the global ocean. If the window is confined to the Atlantic sector of the circumpolar region, then the appropriate longitudinal extent is 6×10^6 m. The maximum longitudinal spread of the windows is the length of the circumpolar region at the latitude of Drake passage: that is, 23×10^6 m. Therefore, our theory predicts that the component of the Atlantic ROC attributable to the adiabatic pole-to-pole cell is between 6 and 23 Sv. This estimate brackets the MOC transport of 18.7 ± 2.1 Sv observed at 26.5°N (Kanzow et al. 2010).

5. Summary and conclusions

In the limit of very weak diapycnal interior diffusion, the net northward heat flux in the South Atlantic Ocean is dominated by a largely adiabatic pole-to-pole overturning circulation, which supplements the contribution from the classical diffusive overturning cells. Our computations show that the necessary ingredients for the existence of an adiabatic pole-to-pole cell are as follows:

(i) A thermally indirect mean circulation in a zonally reentrant channel driven by surface westerlies: Because of the reentrant geometry, the wind drives a deep circulation that overturns the isopycnals, whereas the restratification processes is restricted to mesoscale eddies. Because mesoscale eddies are less efficient than large-scale gyres and meridional currents at transporting buoyancy, this leads to the creation of deep stratification, which provides an adiabatic pathway for deep water to return to the surface.

(ii) A set of outcropping isopycnals that are shared between the channel and the opposite hemisphere:

This allows the opposite hemisphere to act as a source for deep water upwelled in the channel. Because flow occurs along isopycnals, no interior mixing is required. The circulation is closed in the mixed layer, where diabatic processes are plentiful. In contrast, for the isopycnals that outcrop only in the channel, diapycnal flow is required to support the residual overturning circulation (Nikurashin and Vallis 2011).

These requirements are illustrated using a hierarchy of models including a zonally averaged, analytically tractable two-dimensional model; a coarse-resolution numerical model with parameterized eddies; and an eddy-resolving general circulation model.

In the zonally averaged model, the strength and depth distribution of the ROC are determined entirely by the dynamics of the adiabatic interior, enabled by strong diabatic mixing in the mixed layer. In the limit of sufficient mixed layer diabatic processes, the strength of the ROC is independent of the diapycnal diffusivity, a result that we also found in the coarse-resolution model. A finite pole-to-pole ROC can be maintained in the limit of no interior mixing, even for symmetric surface forcing, as long as there is a geometric asymmetry in the form of a reentrant channel in communication with an enclosed basin (modeled here by an asymmetric eddy diffusivity distribution). Although the basin plays some role in determining the stratification, the largest contribution comes from the region where restratification processes are the least efficient (i.e., the channel).

We note that, in the channel, the slope of the buoyancy in the conceptual model is less than that in the coarse-resolution model, although the eddy diffusivity and the surface forcings are the same. This is because in the coarse-resolution and eddy-resolving models the ACC currents deflect into the enclosed portion of the basin, where the wind stress is at a maximum. Thus the relevant forcing is an integral measure of the wind stress over the path of the ACC, taking into account its northward excursion, and this measure is larger than that assumed in the conceptual model (Allison et al. 2010).

The numerical models illustrate the independent effects of the two conditions necessary to support a pole-to-pole component of the ROC. Without a reentrant channel, the middepth stratification and ROC are weak, even if the surface buoyancy forcing is asymmetric (cf. Figs. 3c,f and 5c,f). The presence of a reentrant channel is sufficient to produce strong middepth stratification, but the pole-to-pole component of the ROC is weak unless there is a set of outcropping buoyancy values shared between the Northern Hemisphere and the reentrant channel (cf. Figs. 3a,b,d,e, 5a,b,d,e). The coarse-resolution

simulations more closely approach the limit of zero internal mixing than the eddy-resolving calculations, but the results of the two models are qualitatively very similar. This confirms that the mechanisms determining the pole-to-pole component of the ROC are robust to changes in model dynamics.

In the configuration conducive to the adiabatic pole-to-pole overturning circulation, all three models produce thermostads that we identify with the major water masses associated with the MOC in the Atlantic: Antarctic Bottom Water, North Atlantic Deep Water, and Antarctic Intermediate Water. These thermostads separate the regimes characterizing the interhemispheric geometry of the outcropping buoyancy surfaces: those that outcrop in the ACC region only, those with outcrops shared between the NH and the ACC region, and those that outcrop in both hemispheres but not in the ACC. This characterization needs to be extended to a more realistic equation of state, with temperature and salinity determining buoyancy, and where the geometry of shared outcropping tracers is more complex.

The paradigm for the ROC thus presented implicates the buoyancy and winds in the high latitudes of the Northern and Southern Hemisphere and in particular in the ACC region. However, these two regions compete in their contribution to the ROC [cf. Eq. (28)]: if the westerlies increase in the ACC region, the ''pulling'' of the ROC increases and the ROC strengthens; if the westerlies increase in the high latitudes of the Northern Hemisphere, the ''pushing'' of the ROC decreases and the ROC weakens (cf. Fig. 4). The first effect is well known and has been reported extensively in the literature (e.g., Toggweiler and Samuels 1998; Gnanadesikan and Hallberg 2000; Böning et al. 2008; Klinger and Cruz 2009; Spence et al. 2009), whereas the latter effect has not been previously systematically explored. Similarly, changes in the surface buoyancy in the high latitudes have opposite effects on the ROC: if surface buoyancy is increased in the Northern Hemisphere, the ''window'' of surface densities shared with the ACC region shrinks, slowing down the pole-to-pole cell; conversely, if surface buoyancy is increased in the ACC region, the window of surface densities shared with the Northern Hemisphere expands and the ROC speeds up. Thus, whether the pole-to-pole ROC slows down or speeds up in a changing climate depends on a delicate balance between changes in the ACC region, the Northern Hemisphere, and everything in between.

The sea surface temperature (SST) implications of changes in the pole-to-pole ROC are quite clear: In the Northern Hemisphere, a decrease in the ROC leads to a cooling of SST as the poleward transport of surface waters decreases. In the Southern Hemisphere, the poleward

transport increases, leading to a warming of the SST. These SST changes affect the atmosphere and the cryosphere and need to be evaluated in the context of the coupled system to determine their ultimate effects on the climate.

REFERENCES

Allison, L. C., H. L. Johnson, D. P. Marshall, and D. R. Munday, 2010: Where do winds drive the Antarctic Circumpolar Current? *Geophys. Res. Lett.,* **37,** L12605, doi:10.1029/2010GL043355.

Anderson, R. F., S. Ali, L. I. Bradtmiller, S. H. H. Nielsen, M. Q. Fleisher, B. E. Anderson, and L. H. Burckle, 2009: Wind-driven upwelling in the Southern Ocean and the deglacial rise in atmospheric CO_2. *Science,* **323,** 1443–1448.

Böning, C. W., A. Dispert, M. Visbeck, S. R. Rintoul, and F. U. Schwarzkopf, 2008: The response of the Antarctic Circumpolar Current to the recent climate change. *Nat. Geosci.,* **1,** 864–869.

Cessi, P., and C. L. Wolfe, 2009: Eddy-driven buoyancy gradients on eastern boundaries and their role in the thermocline. *J. Phys. Oceanogr.,* **39,** 1595–1614.

Danabasoglu, G., and J. C. McWilliams, 1995: Sensitivity of the global ocean circulation to parameterizations of mesoscale tracer transports. *J. Climate,* **8,** 2967–2987.

Daru, V., and C. Tenaud, 2003: High order one-step monotonicity-preserving schemes for unsteady compressible flow calculations. *J. Comput. Phys.,* **193,** 563–594.

Ferrari, R., S. M. Griffies, A. J. G. Nurser, and G. K. Vallis, 2010: A boundary-value problem for the parameterized mesoscale eddy transport. *Ocean Modell.,* **32,** 143–156.

Ganachaud, A., and C. Wunsch, 2000: Improved estimates of global ocean circulation, heat transport and mixing from hydrographic data. *Nature,* **408,** 453–457.

Gent, P., J. Willerbrand, T. McDougall, and J. McWilliams, 1995: Parameterizing eddy-induced tracer transports in ocean circulation models. *J. Phys. Oceanogr.,* **25,** 463–474.

Gnanadesikan, A., and R. Hallberg, 2000: On the relationship of the circumpolar current to Southern Hemisphere winds in coarse-resolution ocean models. *J. Phys. Oceanogr.,* **30,** 2013–2034.

Kanzow, T., and Coauthors, 2010: Seasonal variability of the Atlantic meridional overturning circulation at 26.5°N. *J. Climate,* **23,** 5678–5698.

Karsten, R., H. Jones, and J. Marshall, 2002: The role of eddy transfer in setting the stratification and transport of a circumpolar current. *J. Phys. Oceanogr.,* **32,** 39–54.

Klinger, B., and C. Cruz, 2009: Decadal response of global circulation to Southern Ocean zonal wind stress perturbation. *J. Phys. Oceanogr.,* **39,** 1888–1904.

Knorr, G., and G. Lohmann, 2003: Southern Ocean origin for the resumption of Atlantic thermohaline circulation during deglaciation. *Nature,* **424,** 532–536.

Kuhlbrodt, T., A. Griesel, M. Montoya, A. Levermann, M. Hofmann, and S. Rahmstorf, 2007: On the driving processes of the Atlantic meridional overturning circulation. *Rev. Geophys.,* **45,** RG2001, doi:10.1029/2004RG000166.

Liu, Z., and Coauthors, 2009: Transient simulation of last deglaciation with a new mechanism for Bølling-Allerød warming. *Science,* **325,** 310–314.

Lumpkin, R., and K. Speer, 2007: Global ocean meridional overturning. *J. Phys. Oceanogr.,* **37,** 2550–2562.

MacDonald, A. M., S. Mecking, P. E. Robbins, J. M. Toole, G. Johnson, L. Talley, M. Cook, and S. Wijffels, 2009: The WOCE-era 3-D Pacific Ocean circulation and heat budget. *Prog. Oceanogr.,* **82,** 281–325.

Marchal, O., C. Jackson, J. Nilsson, A. Paul, and T. F. Stocker, 2007: Buoyancy-driven flow and nature of vertical mixing in a zonally averaged model. *Ocean Circulation: Mechanisms and Impacts, Geophys. Monogr.,* Vol. 173, Amer. Geophys. Union, 33–52.

Marotzke, J., P. Welander, and J. Willebrand, 1988: Instability and multiple steady states in a meridional-plane model of the thermohaline circulation. *Tellus,* **40A,** 162–172.

Marshall, J., and T. Radko, 2003: Residual-mean solutions for the Antarctic Circumpolar Current and its associated overturning circulation. *J. Phys. Oceanogr.,* **33,** 2341–2354.

McManus, J. F., R. Francois, J.-M. Gherardi, L. D. Keigwin, and S. Brown-Leger, 2004: Collapse and rapid resumption of Atlantic meridional circulation linked to deglacial climate changes. *Nature,* **428,** 834–837.

Munk, W., and C. Wunsch, 1998: Abyssal recipes II: Energetics of tidal and wind mixing. *Deep-Sea Res. I,* **45,** 1977–2010.

Nikurashin, M., and G. Vallis, 2011: A theory of deep stratification and overturning circulation in the ocean. *J. Phys. Oceanogr.,* **41,** 485–502.

Paparella, F., and W. R. Young, 2002: Horizontal convection is non-turbulent. *J. Fluid Mech.,* **466,** 205–214.

Plumb, R. A., and R. Ferrari, 2005: Transformed Eulerian mean theory. Part I: Nongeostrophic theory for eddies on a zonal-mean flow. *J. Phys. Oceanogr.,* **35,** 165–174.

Radko, T., 2007: A mechanism for establishment and maintenance of the meridional overturning in the upper ocean. *J. Mar. Res.,* **65,** 85–116.

Redi, M. H., 1982: Oceanic isopycnal mixing by coordinate rotation. *J. Phys. Oceanogr.,* **12,** 1154–1158.

Rooth, C., 1982: Hydrology and ocean circulation. *Prog. Oceanogr.,* **11,** 131–149.

Sloyan, B. M., and S. R. Rintoul, 2001: The Southern Ocean limb of the global deep overturning circulation. *J. Phys. Oceanogr.,* **31,** 143–173.

Spence, P., O. A. Saenko, M. Eby, and A. J. Weaver, 2009: The Southern Ocean overturning: Parameterized versus permitted eddies. *J. Phys. Oceanogr.,* **39,** 1634–1651.

Stommel, H., 1961: Thermohaline convection with two stable regimes of flow. *Tellus,* **13,** 224–230.

——, and A. B. Arons, 1959: On the abyssal circulation of the World Ocean—II. An idealized model of the circulation pattern and amplitude in oceanic basins. *Deep-Sea Res.,* **6,** 217–218.

Talley, L. D., J. L. Reid, and P. E. Robbins, 2003: Data-based meridional overturning streamfunctions for the global ocean. *J. Climate,* **16,** 3213–3226.

Toggweiler, J. R., and B. Samuels, 1998: On the ocean's large-scale circulation near the limit of no vertical mixing. *J. Phys. Oceanogr.,* **28,** 1832–1852.

Trenberth, K., and J. Caron, 2001: Estimates of meridional atmosphere and ocean heat transports. *J. Climate,* **14,** 3433–3443.

Vallis, G. K., 2006: *Atmospheric and Oceanic Fluid Dynamics: Fundamentals and Large-Scale Circulation.* Cambridge University Press, 745 pp.

Visbeck, M., 2007: Power of pull. *Nature,* **447,** 383.

Weaver, A. J., O. A. Saenko, P. U. Clark, and J. X. Mitrovica, 2003: Meltwater pulse 1A from Antarctica as a trigger of the Bølling-Allerød warm interval. *Science,* **299,** 1709–1713.

Wolfe, C. L., and P. Cessi, 2010: What sets the strength of the middepth stratification and overturning circulation in eddying ocean models? *J. Phys. Oceanogr.,* **40,** 1520–1538.

——, ——, J. L. McClean, and M. E. Maltrud, 2008: Vertical heat transport in eddying ocean models. *Geophys. Res. Lett.,* **35,** L23605, doi:10.1029/2008GL036138.

Wright, D. G., and T. F. Stocker, 1991: A zonally averaged ocean model of thermohaline circulation. Part I: Model development and flow dynamics. *J. Phys. Oceanogr.,* **21,** 1713–1724.